# Physics 357: Fourier Optics

Eliseu Antonio Kloster Filho, Matthew Sinclair, and Maria Fernandez Davila Pastor
(Dated: 11/09/2023)

Analysis of the optical spatial filtering done by a converging, spherical lens was conducted in order to gain a better understanding of the Fourier transform properties of lenses. Using a camera, both transform and image planes were recorded for a beam passing through several different mesh patterns. These pictures were further analyzed and compared against computer generated pictures of Fourier transforms for the same mesh patterns.

## I. INTRODUCTION

Ray optics is a model of optics that describes propagation of light in terms of rays. Such a model is a convenient tool for determining imaging characteristics, including the location of the image and its magnification. In order to achieve a more complete description and deeper understanding of an imaging process, however, it is necessary to consider the wave-like properties of light. Phenomena such as diffraction and interference are responsible for the resolution of optical devices, image contrast, and the effect of spatial filters. In order to take these properties and phenomena into account, it is often useful to think of light, or electromagnetic fields, traveling through free space as a superposition of plane waves propagating at different angles. Looking at these fields through this perspective requires certain mathematical tools like the Fourier transform. The Fourier transform of a field allows us to determine the relative contributions of each of the planes waves in the superposition and, therefore, observe the transmission of each spectral component through the optical system separately. This is usually referred to as the Fourier space representation of the electromagnetic field. More generally, the use of plane-wave decompositions and Fourier transforms in the analysis of optical systems is known as *Fourier Optics*.

### A. Spatial Fourier Transforms

If we consider a two-dimensional object such as a slide which has a field transmission function $f(x, y)$ then this function carries information of the object [1]. An equivalent description of this object in Fourier space is based on the object's amplitude spectrum given by:

$$F(u, v) = \frac{1}{(2\pi)^2} \int \int f(x, y) e^{2\pi i u x + 2\pi i v y} dx dy \qquad (1)$$

Where the variables $u$ and $v$ have units of inverse length and are called the spatial frequencies. $F(u, v)$ is the Fourier transform of $f(x, y)$. If a plane wave of amplitude $E_0$ were to travel through the object, the field distribution immediately behind the object would be $E(x, y) = f(x, y)E_0$, meaning that the object information would be imprinted onto the light wave. There are optical processes that can produce the Fourier transform of $E(x, y)$ and the object function as will be discussed next.

### B. Optical spatial filtering of light

If we think of light traveling through space as a superposition of planes waves, as it is transmitted through a lens, this lens will focus each of the plane waves to a different spot in the focal plane which results in a spectrum of spatial frequencies also known as the Fourier spectrum.

In order to better understand this phenomena, let's consider a plane wave of complex amplitude $U(x, y, z) = Ae^{i(k_x x + k_y y + k_z z)}$ with wave vector $\mathbf{k} = (k_x, k_y, k_z)$, wavelength $\lambda$, wave number $k = (k_x^2 + k_y^2 + k_z^2)^{1/2}$ and complex envelope $A$. The vector $\mathbf{k}$ makes angles $\theta_x = \sin^{-1}(k_x/k)$ with the y-z plane and $\theta_y = \sin^{-1}(k_y/k)$ with the x-z plane. This is shown in Figure 1.

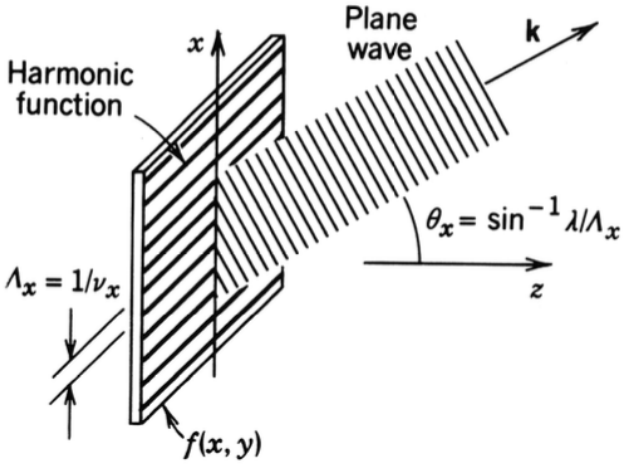


FIG. 1: Plane wave traveling from the left at angles $\theta_x = \sin^{-1}(\lambda v_x)$ and $\theta_y = \sin^{-1}(\lambda v_y)$. Its harmonic function at $z = 0$ has spatial frequencies $v_x$ and $v_y$. Figure sourced from the Lab Guide.

At $z = 0$, the complex amplitude, $U(x, y, 0)$, is a spatial harmonic function $f(x, y) = Ae^{2i\pi(v_x x + v_y y)}$ and with spatial frequencies $v_x = k_x/2\pi$ and $v_y = k_y/2\pi$. Therefore, the angles of the wave vector are related to the

spatial frequencies of the harmonic function by

$$\theta_x = \sin^{-1} \lambda v_x, \theta_y = \sin^{-1} \lambda v_y \tag{2}$$

For this harmonic function, we can recognize the spatial periods to be $\Lambda_x = 1/v_x$ and $\Lambda_y = 1/v_y$ in the $x$ and $y$ directions respectively. If we use these periods to rewrite $\theta_x$ and $\theta_y$, then we can see that these angles depend on the ratios between the wavelength $\lambda$ and the respective spatial period $\Lambda$ (For $\theta_x$ we get an expression of the form: $\theta_x = \sin^{-1}(\lambda/\Lambda_x)$). These geometrical relations follow from matching the wave fronts of the wave to the periodic pattern of the harmonic function in the $z = 0$ plane. In the small angle approximation, $\theta_x \approx \lambda v_x$ and $\theta_y \approx \lambda v_y$ where we can see that these angles of inclination of the wave vector are directly proportional to the spatial frequencies of the corresponding harmonic function.

We can separate the wave plane components in a single wave by using a spherical lens which transforms the plane wave into a paraboloidal wave focused to a point in the lens focal plane. If this wave intersects the lens at angles $\theta_x$ and $\theta_y$, the paraboloidal wave will be centered about a point $(\theta_x f, \theta_y f)$ where $f$ is the focal length as seen in Figure 2. Therefore, the lens focuses each plane wave within the wave onto a specific point in the focal plane, spatially separating each one of them and the contributions of their spatial harmonic functions.

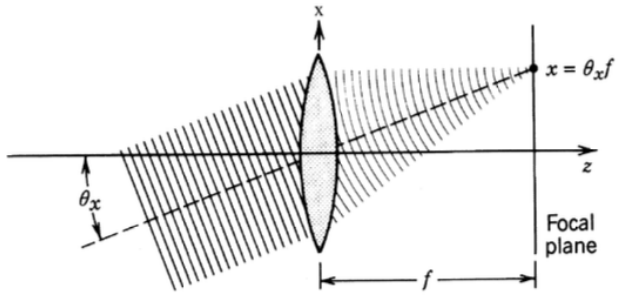


FIG. 2: Representation of the process of focusing a plane wave into a single point on the transform plane. A plane coming in from the left at angles $\theta_x$ and $\theta_y$ is mapped onto a point $(x, y) = (\theta_x f, \theta_y f)$. Figure sourced from the Lab Guide.

Now, let's explore how this spatial filtering occurs in our laboratory setup which is described in Figure 3. An optical wave comes in from the left with complex amplitude $f(x, y, z)$ in the x-y plane. It can be described as a superposition of plane amplitude waves with each wave component traveling at angles $\theta_x = \lambda v_x$ and $\theta_y = \lambda v_y$, and with complex amplitudes proportional to the Fourier transform of $f(x, y, 0)$: $F(v_x, v_y)$.

As they travel through the mesh object and the transform lens, each of these plane wave components is then focused by the lens to a unique point in the focal plane which is at a distance $f$ from the lens. At this point,

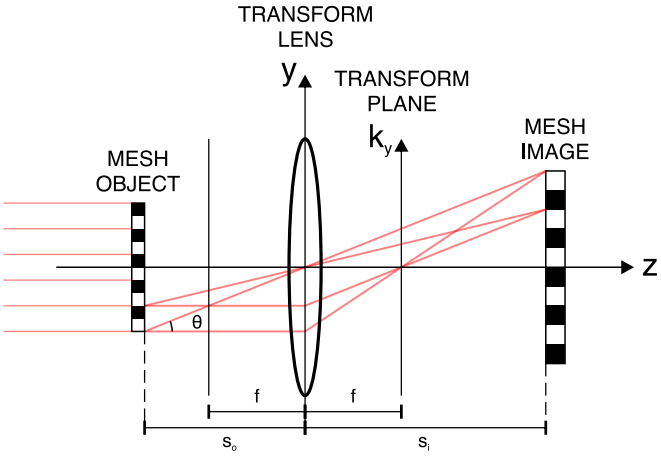


FIG. 3: Visual representation of how the Fourier transform can emerge from a thin converging lens. The transform plane is simply the focal plane of the lens.

the complex amplitude of the wave is proportional to the Fourier transform of $f(x, y, 0)$ evaluated at $v_x = x/\lambda f$ and $v_y = y/\lambda f$ which gives us the following:

$$f(x, y, z = f) \propto F(\tfrac{x}{\lambda f}, \tfrac{y}{\lambda f})$$

The spatial filtering of the beam is performed in the transform plane. This filtering can be of low-pass or high-pass type, and it can also involve selective phase-change of any particular spatial frequency component by using an external filter. A perfect imaging system transmits all spatial frequencies equally, however, using filters with apertures of different diameters would cause certain spectral components to become attenuated which results in a distorted image. They can be used in a clever way can help us remove undesired structures from images and improve the quality of the laser beam.

### C. Inverse Fourier Transform

The inverse of the Fourier transform is naturally performed as the wave keeps traveling in free space from the point where it reaches the transform plane until it reaches the image plane which is a distance $s_i$ from the lens as seen in Figure 2. This inverse transform is what causes the image to be produced at this latter plane. In order to understand this phenomena, we can consider a single point source of light located at the transform plane. This source produces a spherical wave propagating outward with electric field $E = \frac{1}{r} e^{i(kr - wt)}$ where $r$ is the length of the vector pointing from the source to the observation point. We can approximate this spherical wave as a paraboloidal wave where $E \approx \frac{1}{z} e^{ikz} e^{ik(x^2+y^2/2z}$. If the point isn't exactly on the z-axis, but rather at some point off the z-axis $(x_i, y_i)$, then $x$ would become $x - x_i$, and $y$, $y - y_i$. And the electric field produced in the image plane, a distance $d$ from the point emitter emitter on

the transform plane is

$$E(x,y,z) \approx \frac{1}{d} e^{ikd} e^{ik((x-x_i)^2+(y-y_i)^2)/2d} \tag{3}$$

Now, if we consider many of such point sources with similar electric fields, then the electric field observed at the image plane will be the sum of all of these point sources which becomes the integral

$$E(x,y,z) \approx \frac{1}{d} e^{ikd} \int_{-\infty}^{\infty} \int_{-\infty}^{\infty} E(x_i,y_i,z) e^{ik((x-x_i)^2+(y-y_i)^2)/2d} dx_i dy_i$$

In the far field limit, this expression reduces to the Fraunhofer diffraction expression

$$E(x,y,z) \approx \int_{-\infty}^{\infty} \int_{-\infty}^{\infty} E(x_i,y_i,z) e^{-i2\pi(xx_i+yy_i)/\lambda d} dx_i dy_i \tag{4}$$

With this simplified expression of the electric field, we are left with the inverse of a Fourier transform shown in (1) which occurs at the transform plane. However, this is a magnified image where the result rays are diverging, by utilizing a second lens to control such diverging of the rays, then we would be able to observe a more controlled image on the image plane.

### D. Optical Filters

Fourier optics naturally leads to the concept of low- and high-pass filtering in optical systems. So-called *low-pass filters* only permit frequencies above some threshold to pass; frequencies higher than the threshold are blocked. Conversely, *high-pass filters* only frequencies above some threshold through, blocking the lower frequencies.

Optical filtering has many applications in image processing. Low-pass filters, by removing high frequencies, can blur an image and remove unwanted artifacts. Optical high-pass filters act as edge-detectors, facilitating object detection in images. Before the advent of powerful and ubiquitous computers, these image processing tasks leveraged the theory of Fourier optics, using an optical system as an analog computer for Fourier transforms and optical filtering.

Another very interesting application of Fourier optics is in the field of optical computing. This branch of optics was born in the late 20th century, when many scientists dedicated their efforts to the dream of exploiting the incredible speed and parallel properties of light to perform useful calculations. In particular, they aimed to use optical systems as a way of processing information at very high bandwidths [2]. One of the most important results of these investigations is the fact that the fundamental building block of the optical processor architecture is precisely the Fourier transform capabilities of lenses that we study in this lab. More generally, many successful and efficient optical computers have been built [2], including devices with applications in radar signal processing, pattern recognition, and optical memories.

In this lab, we study the Fourier transform performed by a single lens and the corresponding inverse that is carried out by another similar lens. Moreover, we analyze how our resulting images compare to those generated on a computer.

## II. APPARATUS

In order to study the effects of Fourier optics, we constructed a "4-$f$" apparatus capable of optically producing forward and inverse Fourier transforms of laser light. An image of the apparatus is shown in Figure 4, and a simplified diagram can be found in Figure 5.

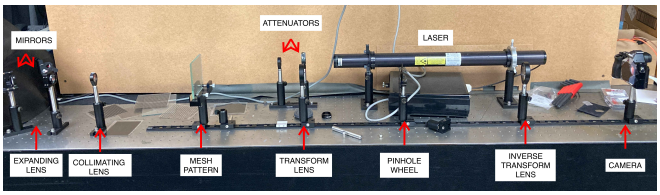


FIG. 4: Picture of the experimental apparatus.

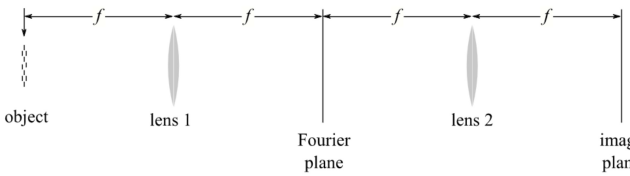


FIG. 5: Simplified diagram of the 4-$f$ apparatus. Beginning on the left, collimated laser light passes through a mesh mask one focal length, $f$, ahead of the first lens. The masked beam then passes through this lens and is focused onto the lens' focal plane, where the Fourier transform appears. The spatial frequency distribution in the Fourier plane becomes the object for a second lens with equal focal length, placed a distance $f$ beyond the Fourier plane. This second lens performs the inverse Fourier transform, reconstructing the image in its own focal plane. Figure sourced from the Lab Guide.

The 4-$f$ apparatus was created in the following fashion. Beginning with a sufficiently powerful source of red laser light, we used spatial filters and a collimating lens to expand and collimate the laser beam, along with alignment mirrors to adjust the beam's direction. When appropriate, we also inserted a filter at this stage to attenuate the beam in order to adjust pixel saturation in the camera.

The collimated beam was then sent through a mesh object. Various meshes were studied, including line gratings (horizontal, vertical, and diagonal), grids of squares, grids of hexagons, and a grid of the Northwestern 'N', among others; Figure 7 shows some of these meshes.

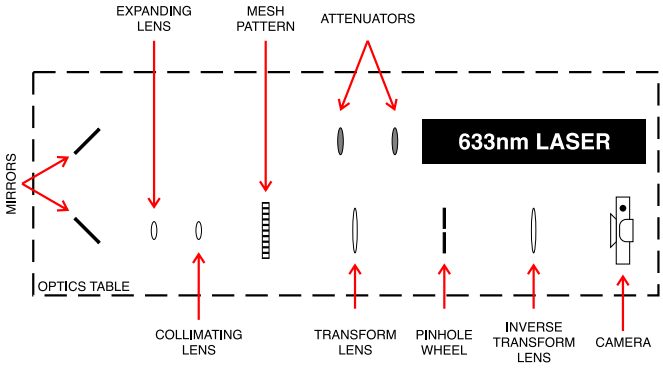


FIG. 6: Schematic diagram of the experimental apparatus.

Each mesh object was a thin sheet onto which a pattern had been printed in black. This partially-opaque pattern blocks portions of the incoming laser light, and therefore the outgoing beam leaves with the profile of the mesh. The location of the mesh is referred to as the object plane.

Located next after the mesh in the path of the beam was a lens of focal length $f = 29 \pm 1$cm. Light sent into this lens is concentrated onto the focal plane a distance $f$ beyond the lens. A second lens, equal in focal length to the first, was positioned one focal length beyond the Fourier plane ($2f$ from the first lens). With these lenses in place, the object, Fourier, and image planes had been established (see Figure 5). A digital camera with a pixel pitch of 8.32 µm was used to photograph the beam at different positions along the apparatus.

The meshes, spatial filters, lenses, and camera were all fixed to bases on a linear optical rail, which allowed for fine positioning and adjustments.

Minor adjustments were made to the apparatus for our two experimental setups.

### A. Predicting features of Fourier transforms

Our first experiment compared observed spatial distances between features in the Fourier plane with distances expected from theory. To accommodate observation of the Fourier transform, we placed the digital camera in the Fourier plane. Horizontal-line grating and square-grid meshes were used as the objects for this experiment, as their Fourier transforms consist of regularly-spaced dots that readily allow comparison to theory.

The segment of the 4-$f$ apparatus beyond the Fourier plane was not relevant for this experimental setup; indeed, the camera necessarily blocked the beam in the Fourier transform plane.

### B. Comparing analog and digital low-pass filters

Our second experimental setup made use of the 4-$f$ apparatus in its entirety. In this experiment, we set out to use a physical low-pass filter to produce blurred images of the meshes and compare the results to those generated digitally on a computer.

To construct an optical low-pass filter, we placed circular holes of varying diameter in the Fourier plane, taking care to align the incident beam to pass orthogonally through the center of the hole. In this way, the parts of the beam farthest from the center (corresponding to the higher frequencies) were blocked. The camera was positioned in the image plane, where it photographed blurred versions of the original mesh.

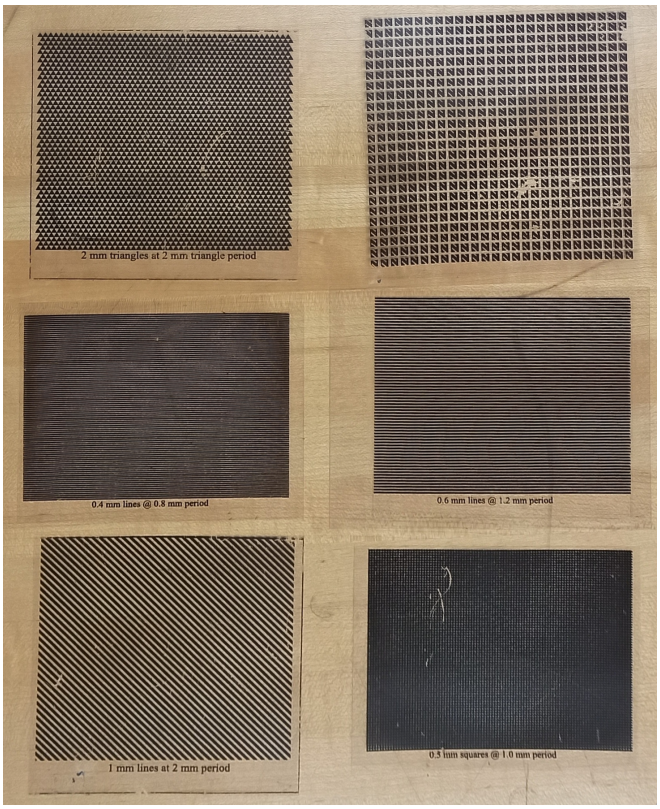


FIG. 7: Six of the meshes used for the low-pass filter experiment. Appearing clockwise from the top left: 2.0mm triangles at 2.0mm period, 3mm Northwestern 'N's at 4mm period, 0.6mm horizontal lines at 1.2mm period, 0.5mm squares at 1.0mm period, 1.0mm diagonal lines at 2.0mm period, and 0.4mm horizontal lines at 0.8mm period.

## III. MEASUREMENTS AND DATA ANALYSIS

### A. Predicting features of Fourier transforms

One of the goals of this experiment was to verify the theoretical expectation that thin lenses act as Fourier transform devices. In this context, some of the simplest mesh patterns were those containing only horizontal lines of constant thickness (as shown in Figure 7). According to our previous discussion in the introduction, each spatial frequency $\nu_x$ should correspond to a dot at $x = \lambda f \nu_x$ in the Fourier plane. Thus, as lines get thicker and more spaced out in the grating plane, we expect the dots in the Fourier plane to get closer together. This is exactly what is qualitatively observed in Figure 8. To get a quantitative understanding of the phenomena, we measured the spacing between all visible consecutive pairs in each of the five mesh patterns. These measurements were averaged and statistical uncertainties were computed from the sample standard deviations. The conversion from pixel units to real world length units was made using the camera's data sheet, which provided a pixel size of $a = 8.32\mu$m. For the theoretical computation, we took $\lambda = 633$ nm, $f = 29 \pm 1$ cm and propagated the uncertainty in the focal length throughout the calculations. Final results are displayed in Table I.

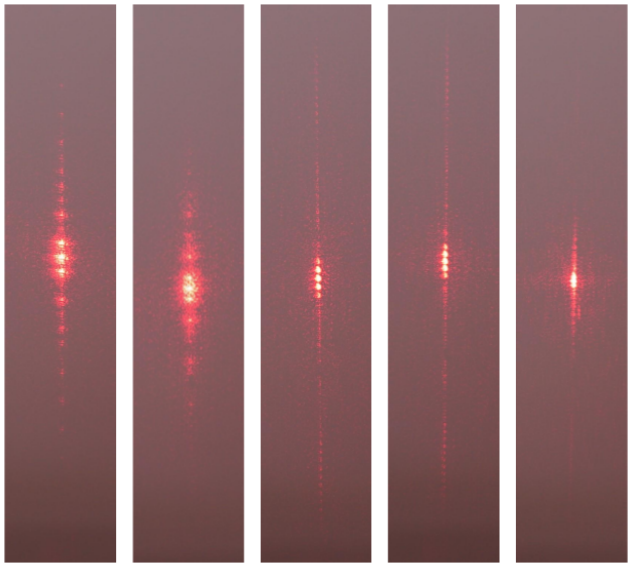

FIG. 8: Photographs taken at the Fourier plane of each of the five horizontal lines grating patterns. From left to right: 0.3 mm lines @ 0.6 mm period; 0.4 mm lines @ 0.8 mm period; 0.6 mm lines @ 1.2 mm period; 1.0 mm lines @ 2.0 mm period. Each individual image is 2.5 mm wide.

We also did the same kind of analysis with a repeating squares pattern. Only one grating of this type was available, so we couldn't investigate a progression of different periods like we did with horizontal lines. Nevertheless, we were able to use this mesh to confirm that the experimental apparatus is indeed capable of producing a 2D Fourier transform. For repeating $0.5 \times 0.5$ mm squares at a $1.0 \times 1.0$ mm period, we expect the horizontal and vertical gap between adjacent dots in the Fourier plane to be $0.183 \pm 0.006$ mm. Experimentally, we obtained a gap size of $0.20 \pm 0.01$ mm. A side-by-side and properly scaled comparison of the grating at the grating plane and at the Fourier plane is shown in Figure 9

| Period (mm) | Gap Size (mm) | Predicted Gap Size (mm) |
|---|---|---|
| 0.6 | $0.31 \pm 0.01$ | $0.30 \pm 0.01$ |
| 0.8 | $0.23 \pm 0.03$ | $0.23 \pm 0.01$ |
| 1.0 | $0.18 \pm 0.03$ | $0.183 \pm 0.005$ |
| 1.2 | $0.15 \pm 0.01$ | $0.152 \pm 0.005$ |
| 2.0 | $0.10 \pm 0.01$ | $0.092 \pm 0.003$ |

TABLE I: Average gap size between consecutive dots in the Fourier plane when compared to the theoretical predictions for all five horizontal lines mesh patterns.

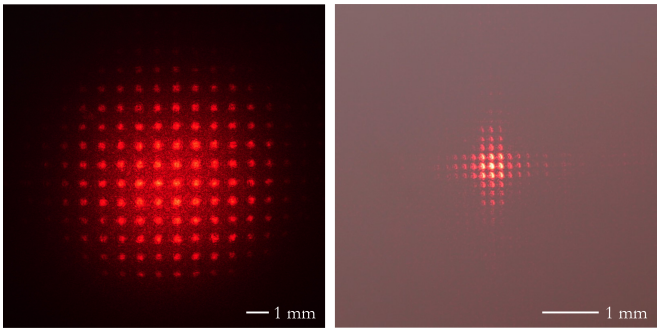


FIG. 9: Side-by-side comparison of the repeating squares mesh (left) and its Fourier transform (right). The mesh consisted of $0.5 \times 0.5$ mm squares at a 1.0 mm period.

As a final step, the percent error between experiment and theory was calculated for the horizontal lines and repeating squares patterns. The results are displayed in Table II.

| Mesh | Percent Error |
|---|---|
| Horizontal/0.6mm period | 2.84% |
| Horizontal/0.8mm period | 0.32% |
| Horizontal/1.0mm period | -2.44% |
| Horizontal/1.2mm period | 3.34% |
| Horizontal/2.0mm period | 6.51% |
| Squares/1.0mm period | 9.90% |

TABLE II: Percent error of the experimentally measured gap size between dots and the theoretical prediction.

### B. Comparing analog and digital low-pass filters

In addition to forward and inverse Fourier transforms, our experimental apparatus has some analog image processing capabilities. This is achieved via manipulation of the image in the Fourier space before it is transformed back to image space. For example, a low-pass filter can be created by restricting the passage of light to a small circular region at the center of the Fourier plane. This effectively prevents the higher-frequency components of the image from being transformed back by the second lens, since they are farther away from the origin. In this experiment, we used a pinhole wheel to control the amount of light that is blocked, which is equivalent to controlling the "strength" of the filter.

The development of advanced image processing techniques is one of hallmarks of modern computation, so it might be surprising to some that even the most simple of these methods could be done with an optical system. To convince ourselves that thinking about our apparatus as a Fourier transform device results in a correct description of what is really happening, we can compare the pictures taken at the Fourier plane with the images obtained from numerically calculating the Fourier transform of each mesh. However, the results can be biased depending on how the original pattern is represented in the computer. For example, defects in the mesh, imperfections in the lenses, and the fact that the laser beam is not a plane wave could interfere with the process. To investigate and account for these effects, we used two different methods to analyze our data. In one of them, we recreated the mesh patterns digitally, which means edges were sharp and no noise was present before the image was transformed. In the other, we provided pictures taken at the mesh plane to the Fast Fourie Transform (FFT) algorithm, so the source data might contain spurious artifacts generated by the camera. On the other hand, it might account for the Gaussian cross-section of the laser beam.

In both cases, we follow the same general procedure to recreate the smoothing effect observed by the camera:

1. Convert the original image (either picture or digital version of the mesh) to a gray scale version.
2. Load it in Python as a 2D-array of floats.
3. Use FFT (as provided by NumPy [3]) to Fourier transform the image.
4. Use the camera's pixel size $a = 8.32\mu$m to convert the units from cycles/pixel to cycles/meter.
5. Frequency shift the result such that the zero frequencies are at the center of the 2D-array.
6. Create a new 2D-array of the same size containing a circular mask in the center. The diameter of the circle in units of cycles/meter $\nu_\Phi$ is related to the diameter of the pinhole in units of meter $\Phi$ by the formula: $\nu_\Phi = \frac{\Phi}{\lambda f}$. Note that if our 2D-array is not square, the circle is actually an ellipse in the cycles/pixel coordinates.
7. Apply the mask to the previously obtained Fourier transform.
8. Frequency shift back and use inverse FFT to transform the 2D-array back into a recognizable image. The output should be a smoothed version of the original.

As an example, we applied this procedure to the Northwestern 'N' pattern exhibited in Figure 7. The results, for both a digital version of the pattern and a photo of the grating are shown in Figure 10. We can see that experiment and theory agree really well, at least qualitatively. This is further evidence that converging lenses can act as Fourier transform devices. Moreover, it serves as an instructional example on the applications of low-pass filters.

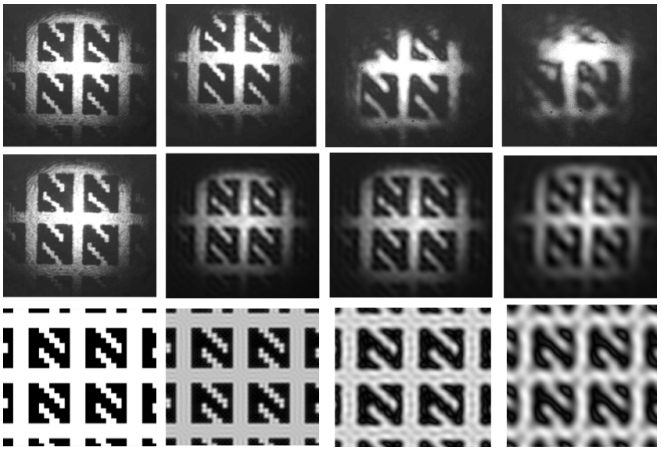

FIG. 10: Observed and simulated low pass filter progressions for a Northwestern 'N' mesh. From left to right, the columns correspond to: no filtering, a hole-filter of diameter 1.0 mm, a hole-filter of diameter 0.5 mm, and a hole-filter of diameter 0.3 mm. The first row contains photographed results from the physical experiment. The second row contains computer-simulated low pass filters based off the unfiltered photograph (note that the first image in both the top and middle rows are therefore the same). The bottom row contains computer-simulated low pass filters based off a computer-generated mesh.

Another interesting example is that of the hexagonal pattern. Since the hexagon has 6-fold symmetry, we should expect the Fourier transform of the hexagonal tiles pattern to exhibit the same kind of symmetry, which is what we observe in Figure 11. To start, we can perform the same kind of analysis that was done for the Northwestern 'N' (which we report in Figure 12). However, because the hexagonal tiles are relatively simple, we can also distinguish the smoothing features by looking at "slices" of each image. For example, Figure 13 shows a slice going through the center of one row of hexagons.

It is then very clear that the low-pass filter is working properly: as the higher frequencies are eliminated, the transitions between outside and inside of the shapes are affected by what is essentially the Gibbs phenomenon.

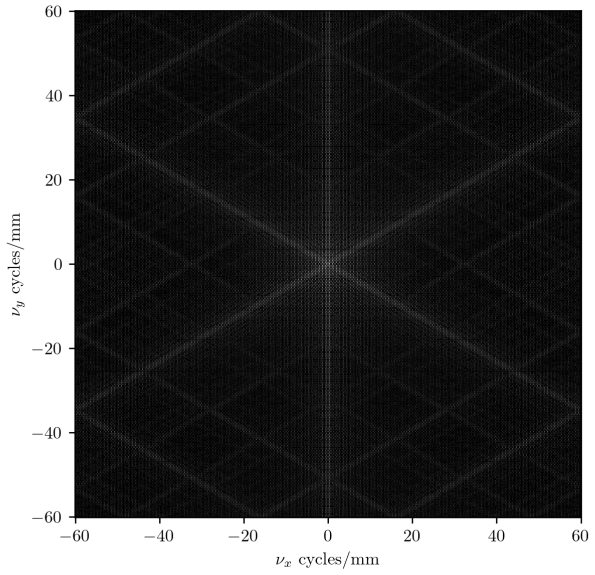


FIG. 11: Fourier transform of a computer-generated repeating pattern of 2.0 mm hexagons at a 3.0 mm period. Note how it has 6-fold symmetry, as expected from the lattice.

Investigating this process using the actual photographs of the pattern before and after filtering is a little more complicated. This is because the pictures are subject to a variety of external effects, including irregular illumination, imperfections in the lenses, the Gaussian cross-section of the laser beam, and other factors that make it such that the differences between the two pictures are not exclusively due to the frequency filtering. Nonetheless, if we do some additional pre-processing to try and mitigate these effects, a similar trend should be expected. Of course, the original picture will not have infinitely sharp edges as its purely digital counterpart has, but we should still be able to see that the edges get softer after the high frequency components are removed. As it turns out, this is exactly what we see in Figure 14.

Qualitatively speaking, we are done. We have shown through cogent arguments that the image formed at the focal plane of a thin converging lens must be the Fourier transform of the object placed in front of it. However, we lack some quantitative evidence to back this claim up. In particular, we would like to quantify the amount of "blurriness" introduced by our pinhole method and compare it to the amount of "blurriness" generated with the computer. This is actually not so hard to do if we restrict ourselves to some key assumptions.

As we have verified experimentally, a more blurred image will contain softer edges. In a review paper, Pertuz et al. argue that a good way of quantifying the "sharpness"

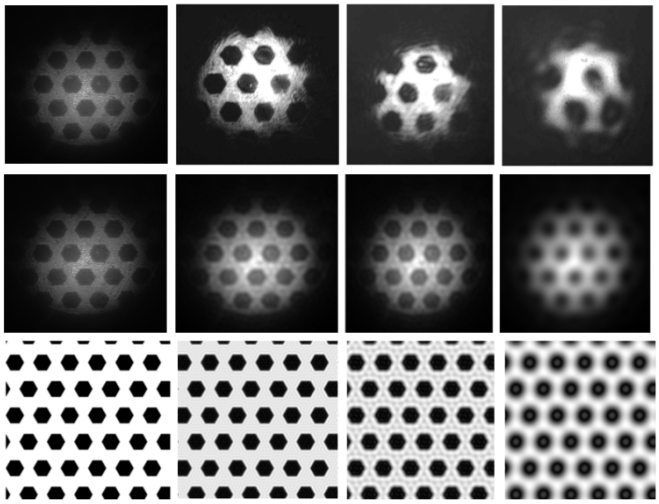

FIG. 12: Observed and simulated low pass filter progressions for the mesh with 2.0 mm hexagons at a 3.0 mm period. From left to right, the columns correspond to: no filtering, a hole-filter of diameter 1.0 mm, a hole-filter of diameter 0.5 mm, and a hole-filter of diameter 0.2 mm. The first row contains photographed results from the physical experiment. The second row contains computer-simulated low pass filters based off the unfiltered photograph (note that the first image in both the top and middle rows are therefore the same). The bottom row contains computer-simulated low pass filters based off a computer-generated mesh.

of the edges is using derivative operators such as the gradient or Laplacian [4]. To determine how blurry the real photographs were compared to the computer predictions, we opted to convolve our images with a Laplacian kernel, represented by the aperture in Equation 5. After the convolution operation, we can compute the variance over the entire resulting image to obtain a single metric that tells us some information about the strength of the low-pass filter applied to it.

$$\mathcal{L} = \begin{bmatrix} 0 & 1 & 0 \\ 1 & -4 & 1 \\ 0 & 1 & 0 \end{bmatrix} \tag{5}$$

This was done for all three of the pinhole diameters that we were able to analyze with the repeating hexagons mesh. The ratio between the real photographs and the computer results was not equal to 1. However, it maintained itself more or less constant for all three pairs of images (see Table III). This means that although we couldn't account for the various external effects at play during the real experiment to obtain a perfect match, we were able to accurately predict how the images change as the diameter of the pinhole changes (at least to within one order of magnitude with a rather simple method).

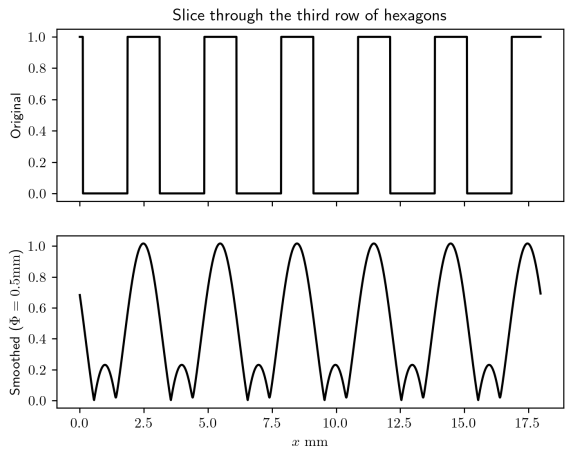


FIG. 13: Comparison between the computer-generated mesh of hexagons and its smoothed version. We took a slice of the image that goes through the center line of a particular row of hexagons in the pattern. Recall that this is the same pattern shown in the third row of Figure 12 and which has its Fourier transform displayed in Figure 11.

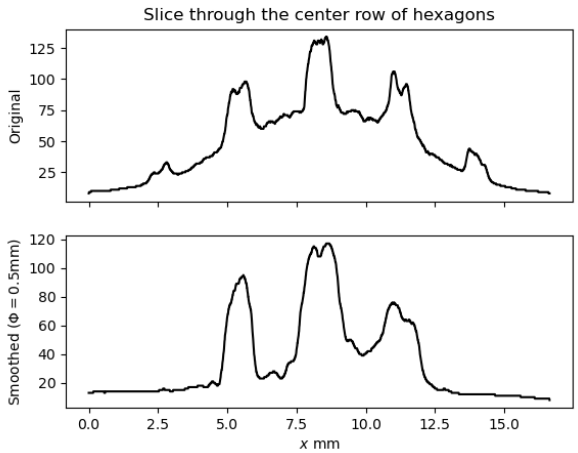


FIG. 14: Comparison between the mesh of hexagons at the grating plane and its smoothed version after going through a pinhole of 0.5 mm diameter. We took a slice of the image that goes through the center line of a particular row of hexagons in the pattern. Note that in the top figure we can observe the Gaussian nature of the beam. Moreover, although barely noticeable because of all the imperfections in the beam, we can see that the bottom figure has its features smoothed out, as expected.

| Φ (mm) | Ratio of the Variance of the Laplacians |
|---|---|
| 0.2 | $3.05 \times 10^5$ |
| 0.5 | $2.37 \times 10^5$ |
| 1.0 | $9.03 \times 10^5$ |

TABLE III: Blurriness metrics for the repeating hexagons. We compute the ratio between the values obtained for the real pictures to the values obtained for the predictions.

## IV. DISCUSSION

Based on the periodic nature of the line-grating and square-grid meshes, we expected to be able to predict features of the optical Fourier transform both qualitatively and quantitatively. Indeed, our results support predictions from theory.

Qualitatively, symmetries apparent in the patterns on the meshes were observed in the corresponding Fourier transforms. For example, the horizontal line-grating pattern, which is by definition invariant under lateral translation, produces an observed Fourier transform that is invariant under vertical translation (see Figure 8; the higher saturation of pixels near the center is due to the finite extent of the beam rather than the Fourier transform itself). Similar symmetries were observed in computer-generated Fourier transforms of our meshes, including the expected 6-fold symmetry of the hexagonal lattice (Figure 11), which serves to validate the computational methods used alongside optical observations.

We have also found agreement with theory in the qualitative investigation of low-pass filters. Our resulting images for meshes blurred with an optical low-pass filter are consistent both with digital transforms done on the initial photograph of the unfiltered beam and with digital transforms performed on computer reproductions of the meshes (Figure 10; Figure 12). Not only do holes of smaller diameter produce progressively blurrier images optically and digitally, but we also find the characteristics of low-pass filtering in our results. For example, ringing artifacts are present in both observed and simulated low-pass-filtered images, perhaps best shown in the third column of Figure 12. And Figure 13 shows the effect of blurring along a one-dimensional slice of a low-pass-filtered image.

Quantitatively, observed average distances between dots in the Fourier transforms of grating patterns fall within the interval expected from theory (Table I; Table II). It should be noted that statistical uncertainties associated with slight differences in the distances between dots in the Fourier plane tended to outweigh systematic uncertainty arising from the measured focal length. Even with a relatively large 1cm uncertainty in the focal length, this systematic uncertainty was at times an order of magnitude smaller than statically uncertainties (e.g. the last row of Table I). This indicates that the observed scale of the optically-produced Fourier transform is perhaps not as sensitive to the positioning of the focal plane as one may expect.

There were some factors that limited the accuracy of the experiment. First, the intensity of the laser often

completely saturated pixels struck by the center of the beam, even when filters were used to attenuate it. Combined with ambient lighting serving to add noise to the results, it was not uncommon for subtler features of some patterns' transforms to be washed away. Moreover, the uncertainty in the focal length of the lenses and spherical aberration may have affected the accuracy of the results. Nevertheless, our results are consistent with theory overall.

## V. CONCLUSION

In this experiment, we applied the theory of Fourier optics to test observations made in a 4-$f$ optical system. We validated theoretical predictions for the Fourier transforms of various mesh objects both by qualitatively observing the appropriate symmetries in optical Fourier transforms and by quantitatively predicting gaps between dots in the observed transforms for line-grating and square-grid patterns. We also investigated the effect of spatial low-pass filters on resulting optical images and found them in agreement with images produced computationally.

For future work, with some combination of a more attenuated beam, more effective camera, or a more controlled environment, it may be possible to investigate the Fourier transforms of some of the more complicated meshes, like the Northwestern 'N' mesh. This could also permit future groups to quantify the root-mean-square difference between observed and simulated transforms with a higher degree of accuracy. And a more precise method of determining the focal length of the lenses could improve the precision of future results.

To enlarge the scope of the experiment in future work, consideration could be given to acquiring more mesh objects to study. A pattern of concentric rings, for example, may provide insight into the effects of its circular symmetry. Allowing custom meshes to be made would also broaden the scope of future work.

Moreover, in this version of the experiment, we did not investigate the effects of optical high-pass filters on the object patterns, since the available disk-filters were far too large and blocked the entirety of the beam. Providing disks of sufficiently small diameter would allow future versions of this experiment to examine the effects high-pass filters along with loss-pass filters.

[1] Miles V. Klein and Thomas E. Furtak. Optics. 1986.

[2] Pierre Ambs. Optical computing: A 60-year adventure. *Advances in Optical Technologies*, 2010:372652, May 2010.

[3] Charles R. Harris, K. Jarrod Millman, Stéfan J. van der Walt, Ralf Gommers, Pauli Virtanen, David Cournapeau, Eric Wieser, Julian Taylor, Sebastian Berg, Nathaniel J. Smith, Robert Kern, Matti Picus, Stephan Hoyer, Marten H. van Kerkwijk, Matthew Brett, Allan Haldane, Jaime Fernández del Río, Mark Wiebe, Pearu Peterson, Pierre Gérard-Marchant, Kevin Sheppard, Tyler Reddy, Warren Weckesser, Hameer Abbasi, Christoph Gohlke, and Travis E. Oliphant. Array programming with NumPy. *Nature*, 585(7825):357–362, September 2020.

[4] Said Pertuz, Domenec Puig, and Miguel Angel Garcia. Analysis of focus measure operators for shape-from-focus. *Pattern Recognition*, 46(5):1415–1432, 2013.